M&C 2017 - International Conference on Mathematics & Computational Methods Applied to Nuclear Science & Engineering, Jeju, Korea, April 16-20, 2017, on USB (2017)

Uncertainty Analysis of Light Water Reactor Core Simulations Using Statistic Sampling Method

Kaiyue Zeng*, Jason Hou*, Kostadin Ivanov*, Matthew A. Jesse†

**Department of Nuclear Engineering, Raleigh, North Carolina, NC 27695-7909*
†Reactor Physics Group, Oak Ridge National Laboratory, Oak Ridge, TN 37831
kzeng2@ncsu.edu, jason.hou@ncsu.edu, knivanov@ncsu.edu, jesseema@ornl.gov

Abstract – *The work presented in this paper is intended to quantify the uncertainty from nuclear data in the Pressurized Water Reactor (PWR) simulation of the Three Mile Island Unit 1 (TMI-1) test case within the OECD/NEA LWR-UAM benchmark framework. The Sampler/Polaris sequence of the SCALE-6.2 system was employed in generating 1000 sets of few group cross sections, which were used in Exercise I-3, the standalone neutronics simulation of the TMI-1 core. The effect of sample size on the simulation accuracy was analyzed and the obtained results show that the sample size of 146 is sufficient to meet the 95%/95% criteria. Investigations on Exercise III-1, the TMI-1 core multi-physics calculation, was performed for the steady-state case using PARCS code with its internal thermal-hydraulic module activated. The distributions for various core key parameters were obtained with associated uncertainties and were analyzed with normality tests. Also studied was the effect of the core composition on the uncertainty of the local power peaking factors.*

I. INTRODUCTION

In order to establish the accuracy and confidence for best estimate codes, the uncertainty in reactor modelling must be quantified. In recent years, the demand to provide best estimate predictions with confident bounds is increasing in the areas of nuclear research, industry, safety and regulation [1]. The uncertainty analysis has been regarded as a significant part in nuclear reactor design and analysis. Consequently, the Organization for Economic Cooperation and Development (OECD) Nuclear Energy Agency (NEA) has launched an international benchmark for uncertainty analysis in modeling (UAM) of light water reactors (LWRs). The goal of this benchmark is to provide an international framework to drive forward the development, assessment, and integration of the comprehensive uncertainty quantification (UQ) methods in best-estimate multi-physics coupled simulations of LWRs during normal and transient conditions [2].

A series of reference systems and scenarios are defined with complete sets of input specifications and experimental data. The benchmark is being carried out in three phases with increasing modelling complexity: Phase I (neutronics phase), Phase II (core phase), and Phase III (system phase). The work presented in this paper is focused on the investigation of the Pressurized Water Reactor (PWR) core modelling with associated uncertainties, specifically for the Three Mile Island Unit 1 (TMI-1) plant for both the standalone neutronics simulation (Exercise I-3) and the multi-physics simulation (Exercise III-1).

II. NUMERICAL TEST CASES

The TMI-1 core contains 177 fuel elements. Each fuel assembly has 208 fuel rods, 16 guide tubes, and 1 tube for the instrumentation. There are 11 types of fuel assemblies in the TMI-1 active core with various fuel enrichment (4.00%, 4.40%, 4.85%, 4.95%, and 5.00%) and configurations with regard to the configuration of the burnable poison (BP) and gadolinia pins (GdO_2+UO_2). The quarter representation is depicted in Fig. 1, where assembly H8 is located at the core center. Detailed geometry setup and material properties can be found in the benchmark specification [3].

	8	9	10	11	12	13	14	15
R	4.85 4Gd	4.95 8Gd	4.85 4Gd	A B C				
P	4.85 4Gd CR(6)	5.00 8Gd	4.40 CR(1)	5.00 8Gd	4.95 4Gd+BP			
O	5.00 4Gd+BP	5.00 4Gd CR(5)	5.00 4Gd+BP	4.95 4Gd CR(3)	5.00	5.00 4Gd		
N	4.40 CR(7)	4.95 4Gd+BP	4.95 4Gd APSR(8)	4.95 BP	5.00 4Gd CR(7)	5.00	4.95 4Gd+BP	
M	4.95 4Gd+BP	4.85 4Gd CR(4)	4.95 4Gd+BP	4.40 CR(5)	4.95 BP	4.95 4Gd CR(3)	5.00 8Gd	
L	5.00 4Gd CR(2)	4.95 4Gd+BP	4.95 4Gd CR(6)	4.95 4Gd+BP	4.95 4Gd APSR(8)	5.00 4Gd+BP	4.40 CR(1)	4.85 4Gd
K	4.95 4Gd+BP	4.95 4GD CR(2)	4.95 4Gd+BP	4.85 4Gd CR(4)	4.95 4Gd+BP	5.00 4Gd CR(5)	5.00 8Gd	4.95 8Gd
H	4.00 CR(7)	4.95 4Gd+BP	5.00 4Gd CR(2)	4.95 4Gd+BP	4.40 CR(7)	5.00 4Gd+BP	4.85 4Gd CR(6)	4.85 4Gd

A – Fuel enrichment, unit: wt.%
B – Gd and BP pin configuration
C – Control rod type and group number

Fig. 1. TMI-1 core layout of fuel assemblies and control rod banks.

For the Exercise I-3, the core condition with the fresh fuel is defined at the hot zero power (HZP) state, where a uniform temperature of 551 K across the core and the moderator density of 0.766 g/cm^3 has been adopted. The specified critical boron concentration is 2600 ppm (parts per million). All control rods were assumed to be fully inserted, including the partial-length axial power shape rod (APSR).

For Exercise III-1, the 3-dimensional (3D) core burnup map has been provided for the beginning of cycle (BOC) and end of cycle (EOC) based on the reactor operational data. The average core exposure is 18 and 40 GWD/MTU at BOC and EOC, respectively. Boron concentration is set to be 1935 ppm and 5 ppm at BOC and EOC, respectively. Two steady state sub-cases, HZP and hot full power (HFP), have been specified. At HZP, control rod groups 1-4 and 5-7 are at the complete withdrawn and insertion positions, respectively, while the APSR is 70% inserted. At HFP, control rod group 1-6 are completely withdrawn, group 7 is completely inserted while APSR is 54% inserted. The thermal-hydraulics (TH) condition of HZP is identical to that in Exercise I-3, while in HFP the inlet moderator temperature is 563 K with a rated power of 2772 MW. The mass flow rate is assumed to be 1.65×10^4 kg/s under system pressure of 15 MPa for all Exercise III-1 cases.

III. METHODOLOGY

In the current study, the only source of uncertainty in the best-estimate calculation under consideration is the nuclear data. The two-group assembly homogenized cross sections based on the ENDF/B-VII.0 were generated using the Polaris code in the SCALE 6.2 [4]. Sampler, a module for statistical uncertainty analysis for SCALE sequences, is used to sample probability density functions (PDF) defined by the SCALE 56-group covariance library and produce random samples of the nuclear data for the Polaris lattice calculations. For the simple random sampling approach, in order to contain 95% of the distribution with 95% confidence, one would be required to sample *N* = 93 times according to Wilks' formula [5]. A recent study on the determination of sample size for more appropriate applications suggested that *N* = 146 to be used to meet the 95%/95% criteria [6]. In order to quantify the influence of the two suggested sample sizes on the calculation results, a large sample size (*N* = 1000) was first adopted in this study and thus 1 nominal plus 1000 perturbed sets of cross sections were generated for each of the 11 fuel assemblies and the 3 reflectors models. The mean and standard deviation of the desired response parameter computed from the reference case was used to construct a perfect normal distribution. The statistical results generated from smaller sample size (*N* = 93 and 146) were then compared with the reference to determine their applicability to this specific application.

The standalone neutronics simulation of the TMI-1 core was performed using the PARCS code [7]. Radially, the core is divided into 21.81 cm × 21.81 cm nodes based on the one-node-per-assembly configuration plus the radial reflector. The axial discretization varies in different exercises and can be found in the following section.

Following the repeated *N* calculations, the resulting distribution of output responses was analyzed with the standard statistical analysis approach by assuming the probability density function (PDF) of output parameter is a normal distribution, which can be characterized by the expected value and standard deviation. Mathematically, the uncertainty in an individual output parameter y can be determined as:

$$\sigma_y = \sqrt{\frac{1}{N-1}\sum_{n=1}^{N}(y_n - \bar{y})^2} \tag{1}$$

where y_n refers to the response to the n^{th} sample input, and $\bar{y}$ denotes the mean value of all *N* responses.

To verify this normality assumption, both graphical tools and quantitative analysis were used as the normality test approach for different output responses, including the core simulation results (e.g., effective multiplication factor k_{eff}, power peaking factors). Graphical representations using histogram plot and probability-probability plot are provided to qualitatively visualize the normality profile. Anderson-Darling goodness-of-fit test, which is a modification of the Kolmogorov-Smirnov test by assigning more weight to the tails of the distribution, are adopted to quantitatively analyze the deviation of the output responses from a perfect normal distribution [8]. This method aims to calculate the A_N^2 value, which represents the distance from empirical cumulative distribution function (ECDF) to the cumulative distribution function (CDF) of a perfect normal distribution and has the following expression:

$$A_N^2 = -N - \frac{1}{N}\sum_{j=1}^{N}(2j-1)\left[\ln(u_j) + \ln(1-u_{N-j+1})\right] \tag{2}$$

where, *N* response data is arranged into the order of $y_1 \le y_2 \le y_3 \cdots \le y_N$. $u_j = F(y_j)$ where $F(y_j)$ is the continuous cumulative distribution function from the corresponding perfect normal distribution. As previously mentioned, the perfect normal distribution is constructed using the same mean and standard deviation as the response distribution and thus $F(y_j)$ could be represented by:

$$F(y_j) = \frac{1}{\sqrt{2\pi}\sigma_y}\int_{-\infty}^{y_j} e^{-\frac{1}{2}\left(\frac{y-\bar{y}}{\sigma_y}\right)^2} dy \tag{3}$$

The hypothesis of normality is rejected if the computed A_N^2 value exceeds the critical threshold of 0.787 [9], or if the *p-value*, which could be interpret as the probability of obtaining an equal or even smaller A_N^2, is less than the predetermined significant level of 0.05.

In this study, the relative uncertainties, namely the ratio of the standard deviation to the mean value, are calculated for some of the important physics parameters, including the lattice multiplication factor k_∞, the core k_{eff}, and power peaking factors.

IV. RESULTS

1. Lattice Calculation

Using the Sampler/Polaris sequence in SCALE 6.2, the lattice calculation for each of the 11 lattice types was repeated for N=1000 required samples to generate the nominal and perturbed cross sections. Due to the limitation in the Polaris modeling capability, the spacer grid cannot be explicitly modelled; instead, an additional cladding has been placed surrounding the fuel rod to account for the effect of the spacer grid.

Table I shows the mean value of k_∞ and its uncertainty for the 11 fuel lattices at HZP with and without taking into account of the spacer grid. The enrichment is denoted by the number following "E". It is reasonable to find the maximum value of k_∞ occurs in the fuel assembly with 5% enriched fuel without the presence of any type of neutron absorber, while the minimum value found in the one with BP and gadolinia pins. The standard deviation of the lattice solution due to nuclear data is about 0.55% for all cases, but higher uncertainties are observed in cases with the neutron absorber.

Table I. Comparison of k_∞ for lattice models with and without spacer grid.

Lattice type	w/ spacer grid	w/o spacer grid
E4.00	1.12780±0.55%	1.12820±0.55%
E4.40	1.15704±0.54%	1.15735±0.54%
E4.85+4GD	1.15748±0.54%	1.15769±0.54%
E4.95+BP	1.06570±0.55%	1.06655±0.55%
E4.95+BP+4GD	1.03814±0.56%	1.03885±0.56%
E4.95+4GD	1.16358±0.53%	1.16377±0.54%
E4.95+8GD	1.13113±0.54%	1.13130±0.54%
E5.00	1.19453±0.53%	1.19471±0.53%
E5.00+BP+4GD	1.04129±0.56%	1.04200±0.56%
E5.00+4GD	1.16657±0.53%	1.16674±0.53%
E5.00+8GD	1.13422±0.54%	1.13438±0.54%

In general, the difference of the lattice solution for models with and without the spacer grid is small as can be seen in both Table I. The Polaris results tends to slightly overestimate k_∞ when ignoring the spacer grid. Although the comparison indicates that the impact of spacer grid on the uncertainty in k_∞ due to nuclear data is negligiable, the spacer grid will still be modelled in the lattice calculation to properly account for its effect on spectrum calculation.

2. Exercise I-3: Core Physics

In this exercise, the full core simulation with only fresh fuel is performed at HZP using the cross sections generated in transport calculations as shown above. In doing so, the uncertainty associated with the nuclear data is propagated from the lattice to the core calculation. The nodal discretization of the PARCS core model consists of 177×16 active nodes and no TH feedback is accounted.

Fig. 2 shows the sample values with the mean and standard deviation of the core k_{eff}. It is observed that the oscillation of the sample mean was reduced significantly after the initial ~150 samples and the standard deviation has also been stabilized. The core k_{eff} is 1.00361 and 1.00340±0.51%, respectively, for the nominal case and over all samples. The relative standard deviation is on the same magnitude of the lattice calculation because only the uncertainty from nuclear data is taken into account, and the neutron leakage at the core level is small such that the infinite lattice is highly similar to the core system.

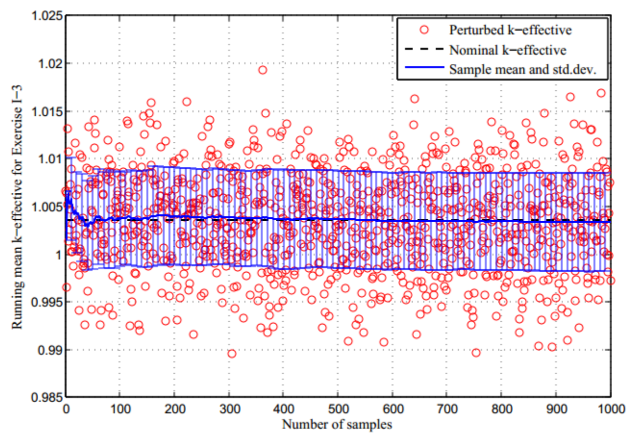

Fig. 2. Sample population for core k_{eff} at HZP condition.

It is a common practice that the response of interest is given by its mean and variance as though the distribution exhibits a normal distribution. It was one of the objectives of the current study to investigate if this assumption is justifiable; therefore, a normality test was first performed for the distributions of core k_{eff}. At Exercise I-3 HZP state, Fig. 3 is a frequency plot of the core k_{eff} combined with a perfect normal distribution, which is characterized with mean and standard deviation derived from the sample output. Fig. 4 is the probability-probability (P-P) plot of the k_{eff} distribution, which can be seen as the cumulative density faction (CDF) of the parameter. Similar trend is observed in Fig. 3 and 4, i.e., the data tend to shrink into the center of the distribution and are sparse at the two tails. Anderson-Darling normality test was then performed for further quantification: the k_{eff} passes the Anderson-Darling test by having an A^2 of 0.428 and a *p-value* of 0.311.

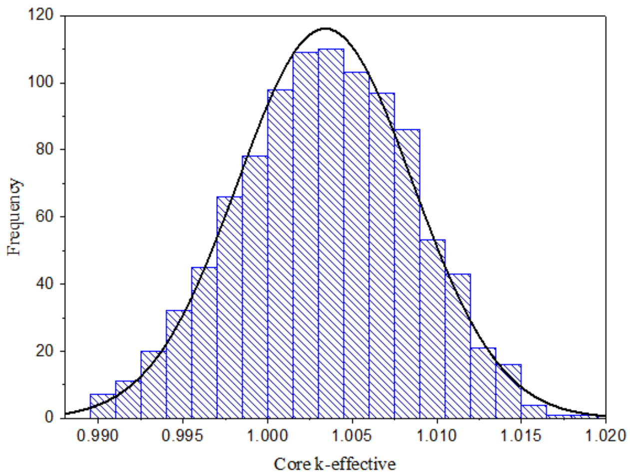

Fig. 3. Exercise I-3 core k_{eff} distribution.

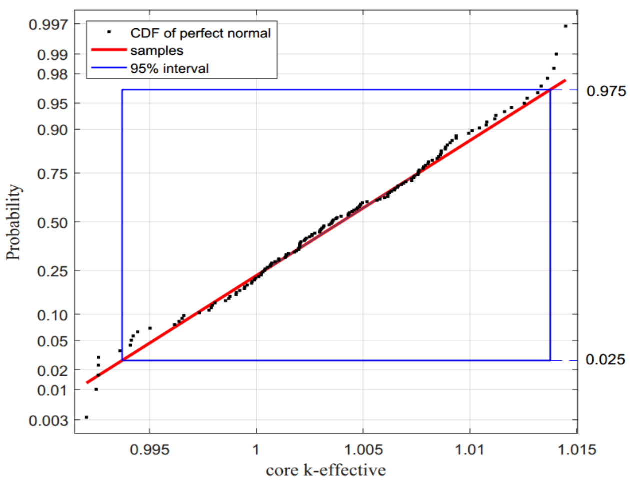

Fig. 4. Probability-probability plot of core k_{eff} for Exercise I-3.

One of the disadvantages of utilizing the statistical sampling method in the uncertainty quantification is its relatively high computational cost. The demand for resources would become even more significant when depletion and the variations of state variables are considered, including the boron concentration, fuel temperature, control rod, and coolant properties etc. It is therefore important to minimize the sample size that is required to maintain certain statistical reliability of the uncertainty analysis. Based on the Wilk's approach, the sample size for double tolerance limits with a 95% of uncertainty and with 95% confidence level is equal to 93 [5]. It was later suggested that the sample size should be at least 146 [6]. In this study, the two critical sample size, N = 93 and N = 146, were examine here to determine whether they meet the 95% percentile with 95% confidence.

The distribution with 1000 samples was used as the reference to construct the a normal distribution with 95% two-sided percentile intervals, i.e., the upper and lower percentile limits are 0.025 and 0.975, respectively. The number of data points exceeding this 95% intervals are then counted for both the N = 93 and 146 distributions, and the fraction of samples inside the 95% interval is calculated and compared to the 95% confidence level. For the core k_{eff}, the 146-sample case yields higher accuracy and 95.2% of the data points are inside the 95% range, while only 92.5% of the data points being bounded in the 95% range for the distribution of the 93-sample case. As a result, the sample size of 150 (approximately 146) has been adopted in the multi-physics core simulation shown in the next section.

Table II shows the power peaking factors in the radial (F_R) and axial (F_Z) direction and their associated uncertainties obtained in Exercise I-3. It should be noted that the peaking location of the radial power distribution is the same for all 1000 samples, but it varies for the axial power map: it occurs at the 9th node from the bottom 87% of the time, while happening at the 10th one for the rest. Consequently, two options were used to report the maximum relative power in the axial direction. The first option is focused only on the maxima among all samples regardless the peaking location, and the second option is to compute the mean and variance of the relative power in node 9. It can be seen in Table II that a smaller uncertainty is found when the peaking location was not taken into consideration. The uncertainty of the radial power peaking factor is found to be 0.55%, which is similar to that of k_{eff}.

Table II. Power peaking factors in Exercise I-3.

F_R	F_Z	F_Z (node 9)
1.683 ±0.55%	1.487 ±0.17%	1.484 ±0.31%

Fig. 5 shows the axial power distribution, which is obtained by normalizing the radially integrated power over each of the 16 axial planes. In the all rods inserted condition, the position of the lower control rod absorber edge from the bottom of the lower fuel rod edge is 14.39 cm for bank 1-7 and 22.32 cm for bank 8. As a result, power at the 1st node is slightly higher than the 16th node. The control rod bank 8 (APSR), consists of an absorber region (156.24 cm) and after that the follower region (186.47 cm). Neutron flux is expected to be higher in the top of the core than the bottom because the rodded portion of APSR is located in the bottom half core. As a result, the axial power distribution is asymmetric and higher in the top. In addition to the mean value, the maximum (red) and minimum (blue) values of the axial power for each plane is also given in Fig. 5. Since the power is center peaked for the fresh fuel at HZP, variations of the axial power profile due to the nuclear data sampling would likely be more pronounced at the lower and upper part of the core, which explains the narrow bound for the central nodes and wider bound for the rest. The axial offset, which is a measure of the difference between power in the top and bottom halves of the core, is found to be 6.60% in this case.

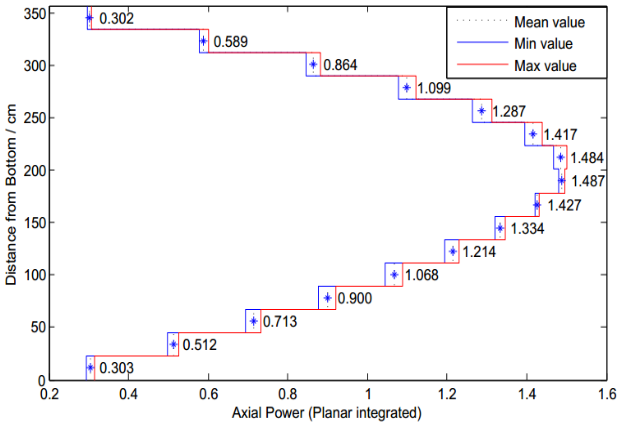

Fig. 5. Exercise I-3 core axial power distribution at HZP.

The assembly-wise power map in the radial direction, including the mean and associated uncertainty, is given in Fig. 6. The maximum value is found to be 1.683 at locations N10 and L12, due to the absence of control rod in neighboring assemblies. The relative standard deviation at these locations is ~0.5%, while that at the core center is over 10 times higher, primarily due to the lower power in the central region.

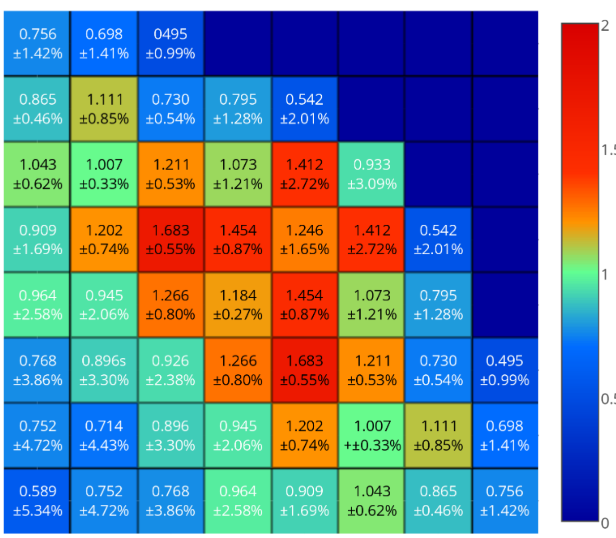

Fig. 6. Ex I-3 core radial power distribution at HZP.

3. Exercise III-1: Core Multi-Physics

In Exercise III-1, 150 burnup dependent sets of cross sections were generated for each of the assembly types. The TH feedback was accounted for using the internal TH module in PARCS. Each of the assemblies is discretized into 24 equal-height computational nodes so as to utilize the 3D core exposure map available in the benchmark specification. Core simulations are done for both HZP and HFP condition, under each condition two subcases, BOC and EOC are considered. A running mean k_{eff} is depicted in Fig. 7 for the HFP state at EOC.

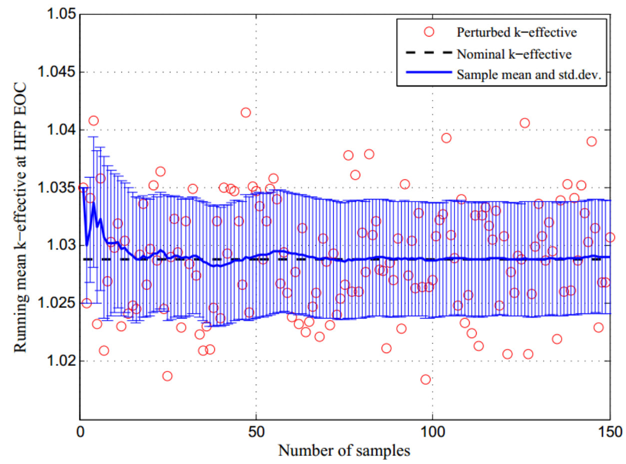

Fig. 7. Running mean k_{eff} for HFP state at EOC.

Table III presents the overall results of the core k_{eff} for the four core states: the mean and standard deviation is given in the second column, while the last two columns showing the outcomes of the Anderson-Darling normality test of core k_{eff}. The core k_{eff} and maximum power peaking factors for all the four states pass the normality test.

Table III. Nominal and sample values of k_{eff} for different states with corresponding Anderson-Darling test results.

State	Nominal k_{eff}	Sample $k_{eff}\pm\sigma$	A^2	*p-value*
BOC HZP	1.01979	1.01986±0.44%	0.624	0.102
EOC HZP	1.04263	1.04276±0.45%	0.379	0.401
BOC HFP	1.01125	1.01136±0.46%	0.748	0.050
EOC HFP	1.02885	1.02902±0.47%	0.397	0.364

A summary of maximum radial and axial power peaking factors derived from 150 sample runs are provided in Table IV with uncertainties included. The uncertainties are within 5% and relatively high uncertainties are observed at HZP condition, especially, uncertainties at HZP EOC state is observed to be relatively larger than the values at other states.

Table IV. Key core physics parameters.

State	F_R	F_Z
HZP BOC	1.702±2.34%	1.346±0.13%
HZP EOC	2.172±1.21%	1.793±4.56%
HFP BOC	1.351±0.98%	1.408±0.33%
HFP EOC	1.437±1.04%	1.243±0.75%

The example representation of the core k_{eff} frequency histogram and the corresponding P-P plot is made for the HFP core at EOC, as shown in Fig. 8 and 9, respectively.

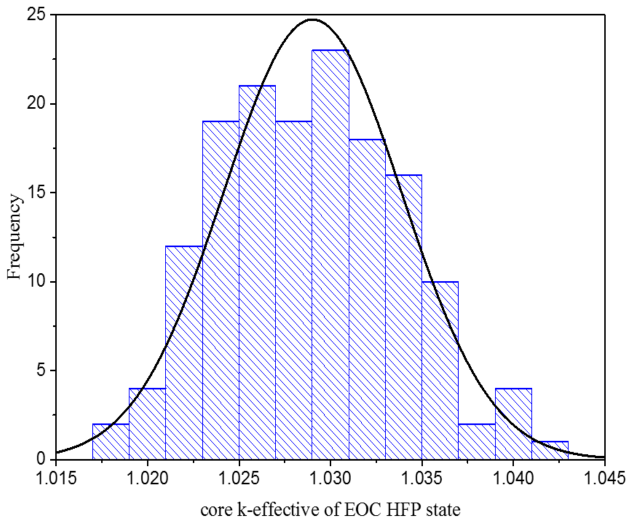

Fig. 8. Exercise III-1 HFP core k_{eff} distribution at EOC.

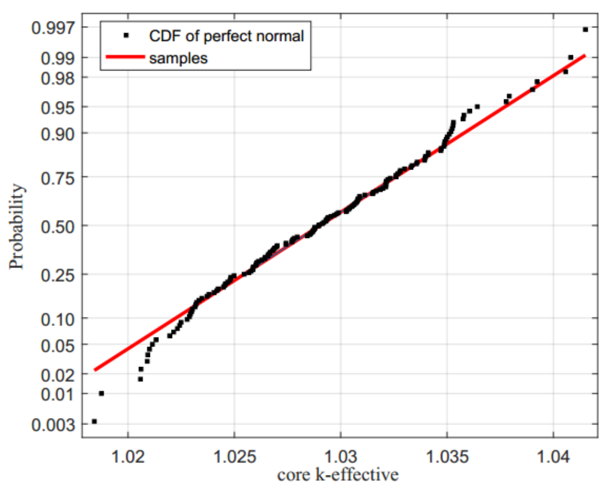

Fig. 9. Probability-probability plot for core k_{eff} at EOC HFP.

Anderson-Darling test was also performed for the power peaking factors. Similar to the previous exercise, the peaking location in both radial and axial power distribution may vary sample by sample; therefore, the peaking factor has been reported following two approaches as shown in Table V. In the first method, denoted as M1, the peaking factor distribution was constructed from maximum relative power taken from the core results regardless the peaking location. In the second method (M2), the peak location was identified first based on the mean power distribution over all samples, followed by the peaking factor selected and used to form the distribution.

It is found that for the BOC HFP case, the maximum relative power was observed at location K10 and L9 51% of the time, while at L11 and M10 for the rest. As a result, the maximum relative power is not normally distributed anymore if the M1 approach is adopted due to the different assembly compositions at locations K10 and L11. Although axial power could also peak at different locations, the locations for different samples were closed to each other and the cross sections for nearby axial locations do not differ significantly.

Table V. A^2 and corresponding *p-values* for power peaking factors at various core states.

	State	F_R (M1)	F_R (M2)	F_Z (M1)	F_Z (M2)
A^2	BOC HZP	0.223	0.195	0.447	0.443
	EOC HZP	0.261	0.261	0.244	0.275
	BOC HFP	**2.308**	0.500	**1.219**	0.282
	EOC HFP	0.479	0.479	0.272	0.313
p-value	BOC HZP	0.819	0.890	0.277	0.284
	EOC HZP	0.702	0.702	0.760	0.655
	BOC HFP	**<0.005**	0.206	**<0.005**	0.635
	EOC HFP	0.232	0.232	0.666	0.544

Fig. 10 represents the axial power profile at HFP. The fuel in the middle of the core is burnt at a higher rate than that at the axial ends at HFP, which leads to the reduction of axial peaking factor over the cycle, as shown in Fig. 10.

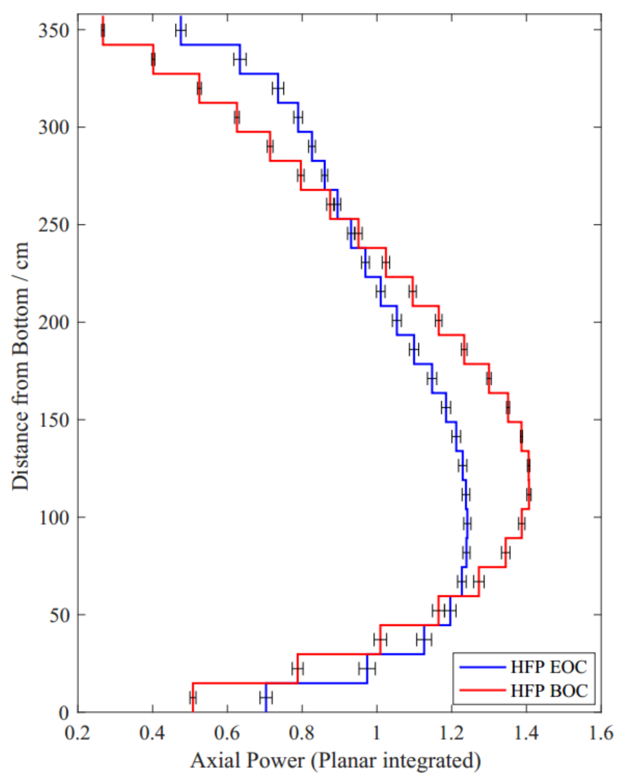

Fig. 10. HFP axial power profile.

Fig. 11 represents the axial power profiles at HZP states. At HZP, the temperature is uniform everywhere and axial depletion dominates the axial power shape. The absolute axial difference between average depletion in the top and bottom halves of the core is found to be 9.78

GWD/MTU at BOC, while this value is 19.36 GWD/MTU at EOC. As a result, the HZP axial power peaks pronouncedly at top half of the core at EOC compared to that at BOC as shown in Fig. 11.

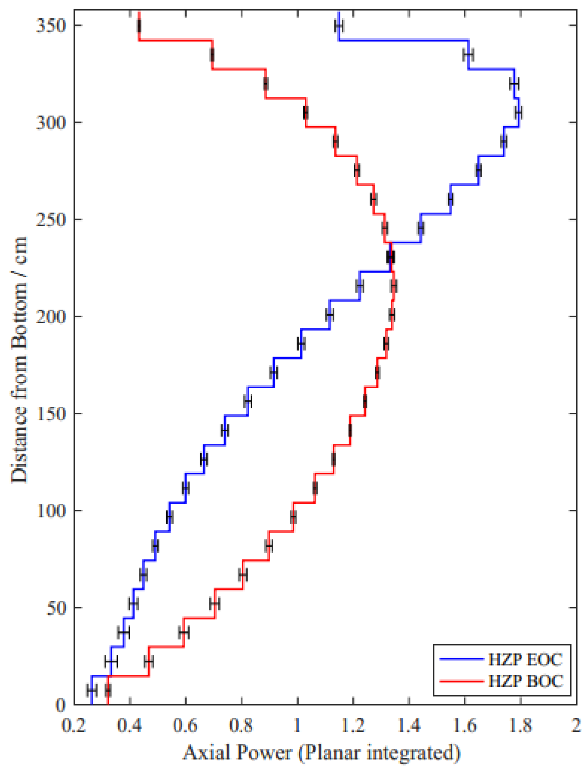

Fig. 11. HZP axial power profiles.

Higher relative uncertainties of axial nodal power at the bottom and top of the core were observed as shown in Fig. 10 and 11, which is due to the fact that the mean power at those regions are lower compared to that at the core center.

Figs. 12-15 depict the radial assembly power distributions derived from the 150 sample runs for different core states. The maximum radial assembly power were found to be in the same location comparing the two HFP states. In general, the lowest power was found at the central assembly in all cases because control rod bank 7 was inserted in all the states. The maximum radial power were found to be in positions where a control rod inserted in the neighboring assemblies.

It was found that the assembly composition has a large impact on the uncertainty of the assembly power. For example, larger uncertainties were observed at BOC than that at EOC for both HZP and HFP states. In addition, it was found that the uncertainties of HZP is more pronounced than that of the HFP, probably because at HZP two more control rods banks (bank 5 and 6) are inserted into the reactor core and higher uncertainties are introduced as a result.

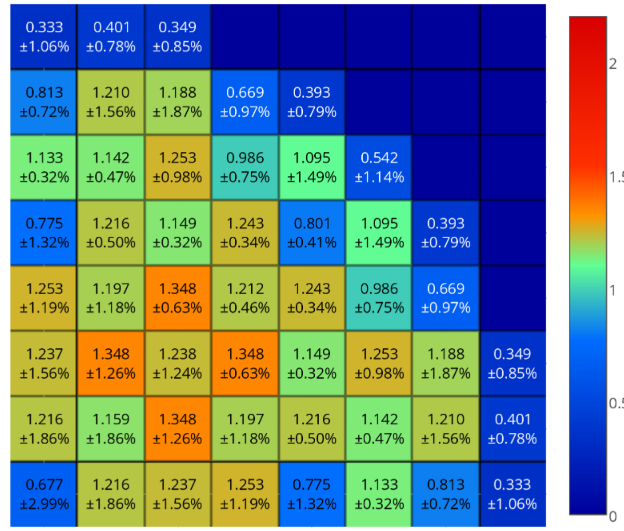

Fig. 12. HFP radial power distribution at BOC.

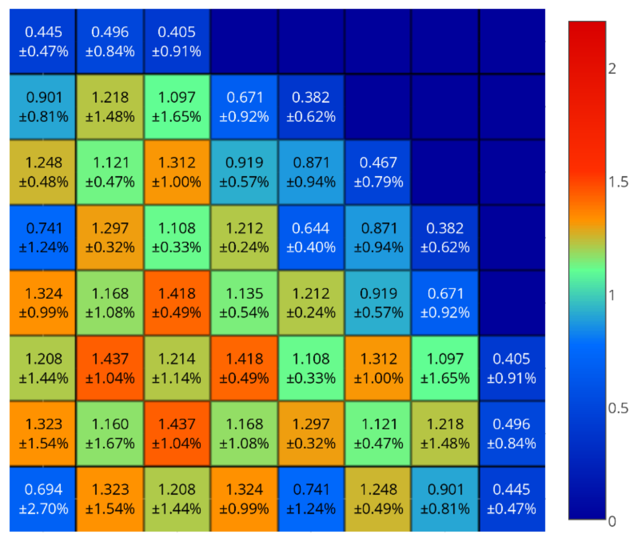

Fig. 13. HFP radial power distribution at EOC.

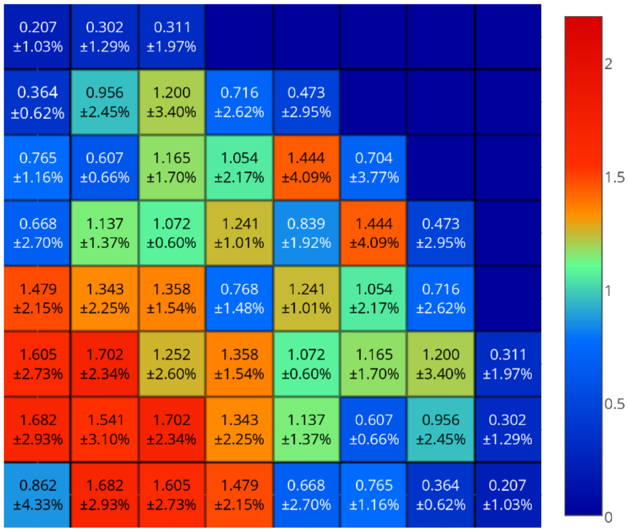

Fig. 14. HZP radial power distribution at BOC.

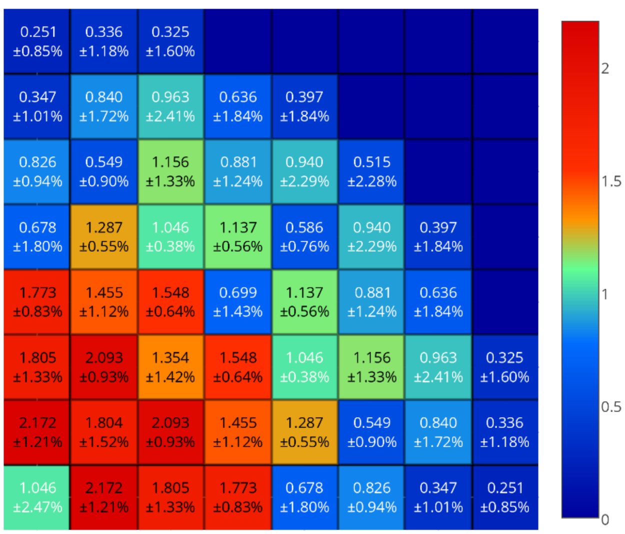

Fig. 15. HZP radial power distribution at EOC.

V. CONCLUSIONS

This paper presents the results of the uncertainty analysis for the TMI-1 core steady-state simulation within the framework of the LWR UAM benchmark by taking into account the uncertainty from the nuclear data using the statistical sampling approach. The Sampler/Polaris sequence was used for the nuclear data sampling and few-group cross section generation, and the core simulation was done using PARCS.

In the standalone neutronic calculation (Exercise I-3), it was shown that the k_∞ of the lattice results exhibits a normal distribution with the relative standard deviation of ~0.5% in all lattice cases. As the uncertainty were propagated to the reactor core level through the few-group constants, no noticeable increase in the relative standard deviation was found, as the effective multiplication factor was 0.51%. Normality test shows that the core k_{eff} is well represented by the normal distribution. A brief study of the sample size shows that the 146, instead of 93, should be used in order to meet the 95%/95% criteria. As a result, 150 runs were performed for following calculations.

In the multi-physics core calculations (Exercise III-1), the TH feedback was provided by the internal TH module in PARCS. Four sub-cases, HZP BOC, HZP EOC, HFP BOC, and HFP EOC were simulated and similar analysis was conducted as in the previous exercise. Slightly smaller uncertainties were observed for the core k_{eff} compared with that in the standalone result. For maximum radial assembly power, the uncertainties of HZP tend to be larger than those of HFP. It was observed that the uncertainty of radial assembly power was larger at BOC when compared with that at EOC. Normality tests show that both the core k_{eff} and power peaking factors can be represented by the normal distribution, except for cases where the power peaking locations were ignored.

REFERENCES

1. K. Ivanov, et al., "Uncertainty Analysis in Reactor Physics Modeling," *Science and Technology of Nuclear Installations*, vol. 2013 (2013).
2. F. Díauria, et al., "Technology Relevance of the "Uncertainty Analysis in Modelling" Project for Nuclear Reactor Safety," NEA/NSC/DOC (2007).
3. K. Ivanov, et al., "Benchmark for Uncertainty Analysis in Modeling (UAM) for Design, Operation and Safety Analysis of LWRs," NEA/NSC/DOC (2016).
4. B. Rearden, et al., "SCALE Code System," Oak Ridge National Laboratory (2016).
5. S. Wilks, "Determination of Sample Sizes for Setting Tolerance Limits," *The Annals of Mathematical Statistics*, vol. 12 (1941).
6. In Seob Hong, et al, "Generic Application of Wilks' Tolerance Limit Evaluation Approach to Nuclear Safety," NEA/CSNI/R (2013).
7. T. Downar, et al., "PARCS v3.0 U.S. NRC Core Neutronics Simulator User Manual," University of Michigan (2012).
8. T. W. Anderson, D. A. Darling. "A test of goodness of fit," *Journal of the American Statistical Association*, vol. 49, no. 268, pp. 765-769 (1954).
9. M. A. Stephens, "EDF Statistics for Goodness of Fit and Some Comparisons," *Journal of the American Statistical Association*, vol. 69, pp. 730–737 (1974).
10. A. R. Henderson, "Testing experimental data for univariate normality," *Clinica Chimica Acta*, vol. 366, pp. 112-129 (2006).